Flagellotropic bacteriophage selects for evolutionary remodeling of cell motility and chemotaxis in *Escherichia coli*

Short title (50 characters):

Phage Selection Remodels Bacterial Motility

Jyot D. Antani[1,2,3,✉], Austen Theroux[1], Fotios Avgidis[3,4], Birgit E. Scharf[5], Thierry Emonet[3,4,6], Paul E. Turner[1,2,3,7,✉]

[1]Department of Ecology and Evolutionary Biology, Yale University, New Haven, CT 06520, USA

[2]Center for Phage Biology & Therapy, Yale University, New Haven, CT 06520, USA

[3]Quantitative Biology Institute, Yale University, New Haven, CT 06520, USA

[4]Department of Molecular, Cellular and Developmental Biology, Yale University, New Haven, CT 06520, USA

[5]Department of Biological Sciences, Virginia Tech, Blacksburg, VA, 24061, USA

[6]Department of Physics, Yale University, New Haven, CT 06520, USA

[7]Program in Microbiology, Yale School of Medicine, New Haven, CT 06520, USA

✉ Co-corresponding author emails/ORCiDs:

jyot.antani@yale.edu / 0000-0002-7402-983X;

paul.turner@yale.edu / 0000-0003-3490-7498

Keywords

phage-bacteria interactions, flagella, motility, chemotaxis, evolution

Teaser (125-character summary)

Evolution redesigns bacterial swimming and navigation to escape viruses while maintaining motility in complex environments.

Abstract

Bacteria can evolve resistance to bacteriophage attack via mutations that alter phage receptors on the cell surface. Flagellotropic phages bind to motility-enabling flagella, creating an evolutionary trade-off, since losing flagellar function reduces fitness in many environments. We experimentally evolved *Escherichia coli* populations under selection by flagellotropic phage χ (chi), on soft-agar swim plates which favor motility. Whole genome sequencing revealed early emergence of non-motile mutants with disrupted motility-genes, followed by motile mutants with flagellin gene mutations. Swim-plate assays and single-cell tracking showed variable motility effects among resistant mutants, with some faster and others slower than ancestors. Increased tumble bias suggested altered flagellar rotation. Kinase-response in the upstream chemotaxis pathway was also remodeled in χ-resistant mutants. Our findings demonstrate that evolved phage-resistance can cause motility to trade-off or trade-up, revealing diverse evolutionary outcomes under combined selection pressures.

Introduction

Bacteriophages (phages), the viruses of bacteria, have existed alongside their bacterial hosts for perhaps billions of years. Following infection and intracellular replication of bacteria, lytic phages destroy (lyse) host cells to release virus progeny, thereby imposing strong selection for bacterial populations to evolve defenses against phage attack[1,2]. Bacteria can evolve phage-resistance by mutating or suppressing the phage binding receptor(s) on the cell surface, because viruses use the structure(s) to initiate infection. Phages have evolved to exploit various exposed structures on host cell surfaces for attachment, including transmembrane channels, saccharides, and appendages. Binding to appendages that extend well beyond the cell surface may increase the probability of freely-diffusing phages to collide with such structures on host cells suitable for infection[3,4].

Flagellotropic phages infect bacteria by first interacting with the bacterial flagellum[5]. Flagella are threadlike extracellular appendages that sometimes extend up to multiple cell lengths. Rotation of flagella enables planktonic motility of bacteria in aqueous media as well as their swarming motility on semisolid surfaces[6]. Obstruction of flagellar rotation is thought to be the earliest signal in surface sensing by bacterial cells[7–9]. Flagellar motility allows bacteria to efficiently explore their environments through chemotaxis (directed movement along chemical gradients)[10], and differing motility can determine relative fitness (reproduction success) of bacterial variants (genotypes) in a population when movement is essential for obtaining limiting nutrients[11,12] and is considered a virulence factor for certain bacterial pathogens[13]. If mutations arise in the motility apparatus of bacteria to evade attack by flagellotropic lytic phages, movement through the environment may be negatively affected, thus representing a crucial fitness trade-off suffered by bacteria that evolve phage resistance. While bacteria and flagellotropic phages are thought to coexist in nature[5,14], the mechanisms by which bacteria evolve resistance against such phages remain poorly understood[12].

Bacterial motility and chemotaxis in *Escherichia coli* have been extensively studied over the last five decades[15–18]. Cells express multiple flagella distributed across the cell, each with a transmembrane flagellar motor at its base. The left-handed flagella bundle together when rotating in their default counterclockwise (CCW) direction and propel the cell forward, resulting in straight ‘runs’. When one or more motors switch to clockwise (CW) rotation, the bundle breaks, and the cell reorients due to forces in different directions, resulting in a ‘tumble’. Through run-tumble motility, cells perform a random walk that is biased toward CW rotation (tumbles) through binding of an intracellular motor-response regulator CheY-P to the motor. This regulator is part of the

chemotaxis two-component system, in which the kinase CheA, when activated, phosphorylates CheY. CheA localizes at a cellular pole along with the receptor array, which can sense extracellular ligand concentrations and accordingly modulate CheA activity. Another chemotaxis enzyme, CheZ, acts as a phosphatase for CheY-P.

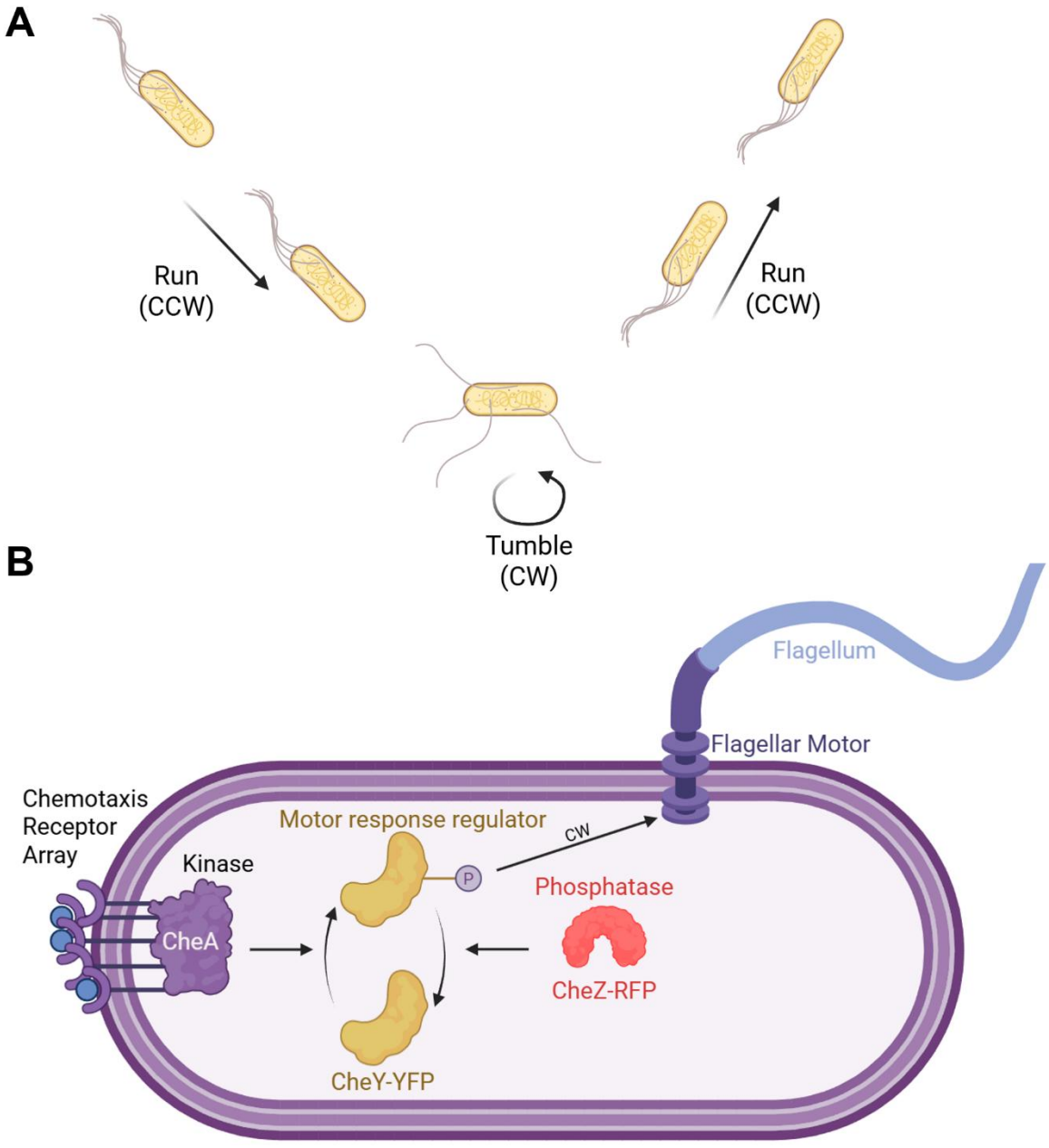

Fig 1. Flagellar motility and chemotaxis in *Escherichia coli*. (A) Flagella bundle together when rotating counterclockwise (CCW) and push the cell in a straight 'run'. When one or more flagella turn clockwise (CW), the bundle breaks and the cell reorients, which is termed a 'tumble'. Switching between runs and tumbles allows cells to navigate their environment. **(B)** The chemotaxis network controls the rotational

direction of the flagellar motors through a two-component system. Receptors sense ligand molecules and accordingly adjust the kinase CheA's activity. The activated kinase phosphorylates the response regulator CheY, while the phosphatase CheZ can dephosphorylate it. Förster Resonance Energy Transfer (FRET) between CheY-YFP and CheZ-RFP provides a readout of kinase activity.

Here, we used experimental evolution to examine whether populations of *E. coli* could maintain motility while evolving resistance against the virulent phage χ, a model flagellotropic phage. Phage χ requires fully functional, rotating flagella for successful infection[19,20]. We conducted experimental evolution of bacterial populations founded by the motile *E. coli* strain MG1655 in replicated environments containing both phage selection pressure and positive selection for cell motility. Early in the experimental evolution, whole genome sequencing revealed that nonmotile χ-resistant mutants featured deletions in motility and chemotaxis genes, mediated by the transposon IS1 (insertion sequence 1). Whereas, later in evolution, phage-resistant mutants maintained motility and carried mutations in *fliC*, the gene encoding flagellin, which is the primary component of the flagellar filament. We observed parallel evolution across treatment populations of specific key mutations that impart single amino-acid substitutions affecting the outer D3 domain of flagellin. Finally, we assessed the evolutionary impact of key mutations on bacterial motility and chemotaxis using swim-plate assays, single-cell motility tracking, and FRET (Förster Resonance Energy Transfer)-based measurements of chemotaxis kinase activity[21,22] (**Fig 1**), by comparing the ancestral strain to its evolved descendants, including control strains evolved in absence of phage χ. This study highlights the molecular adaptations and evolutionary outcomes experienced by populations of motile bacteria when selected to maintain motility while avoiding infection by a flagellotropic phage.

Experimental Evolution Overview

Typical phage-bacteria coevolution experiments involve co-culturing phages and bacteria in shaking flasks with serial transfers (dilution bottlenecks into a flask containing fresh medium) performed every ~24 h. Flagellar synthesis and operation are often energetically expensive: flagellar synthesis may account for ~2% of the total cellular energy expenditure in model strains of *E. coli* and *Salmonella* and up to ~10% in non-model bacteria[23,24]. When an anti-flagellar evolutionary pressure such as phage χ is present, bacterial mutants with defective flagellar synthesis may emerge as a simple adaptive strategy. In more natural and complex environments, however, bacteria must also maintain motility to locate nutrient-rich habitats. To simulate these conditions, we challenged *E. coli* to evolve under laboratory environments alongside phage χ while also selecting for bacterial motility. To do so, we introduced a high concentration of χ-phage

into 'soft' agar (0.3%), containing a tryptone-based growth medium that allows bacteria to move via chemotaxis-driven flagellar motility. We then inoculated bacteria from a freshly-grown culture of motile *E. coli* MG1655 (defined as ancestor or wild-type) in the center of the soft-agar plate and incubated it for up to 48 h at 30°C. The expectation was that motile bacteria would spread concentrically through the medium, expanding in population size to create a visible 'swim' ring, whereas non-motile bacteria would remain near the center of the agar plate, because they were unable to move. Serial passage (1:2000 population bottlenecking) was achieved by harvesting the plate contents, mixing 1:1 with liquid medium, and using a dilution of this mixture to repeat the process of inoculating the bacteria into the center of a fresh soft-agar plate containing phage χ. Samples from harvested plates were used to create frozen stocks that were stored for later analysis. This process was repeated for 10 passages total, for each of 10 independently evolving replicate lineages (Treatment lineages T1 through T10) descended from the original ancestor genotype (**Fig 2**). This method favored evolution of χ-resistant bacteria that were additionally selected to maintain flagellar motility. In addition, four control lineages (C1 through C4) were serially passaged identically, using plates where phage χ was absent.

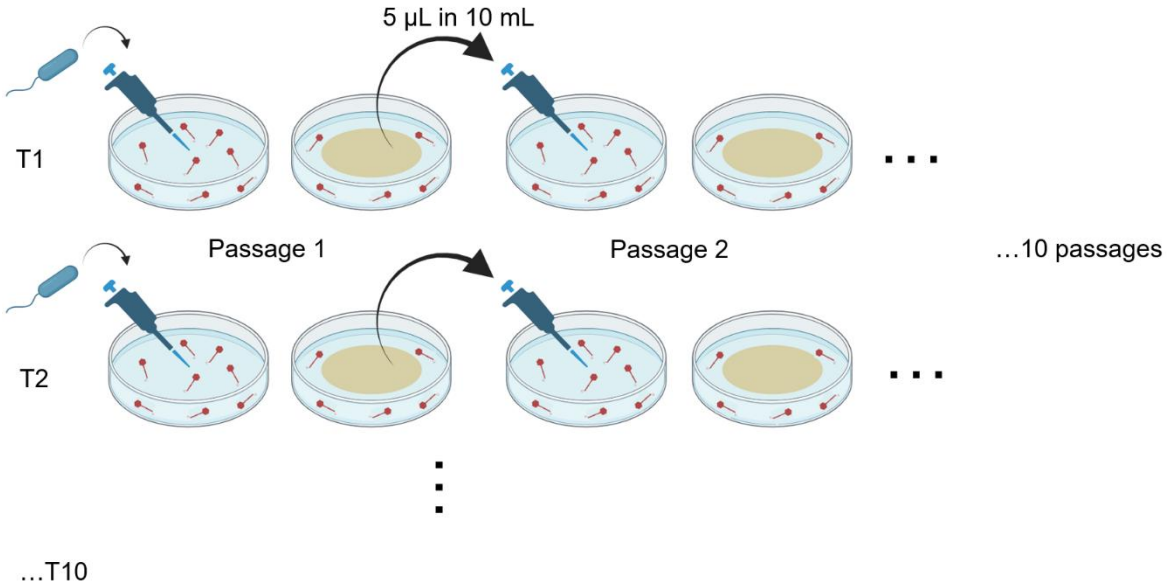

Fig 2. Swim-plate assay for evolution of bacteria against χ-phage. We inoculated bacteria into the center of swim plates (0.3% agar) embedded with phage χ. After 24-48 hours of incubation at 30°C (one passage), we transferred an aliquot to fresh plates containing phage χ. We continued this protocol for 10 passages, for 10 independently evolving replicate Treatment lineages T1-T10, and for four Control lineages C1-C4 evolved in absence of phage χ (not shown).

Results

IS1 insertions mediate resistance to phage χ in early evolved, nonmotile mutants

Early in the evolution experiment, we observed that bacteria in all 10 Treatment lineages (up to passage 2 in some lineages, up to passage 3 or 4 in others) failed to form a swim ring even after 48 hours of incubation. Instead, non-motile cells grew on the plate as isolated, 'spotty' colonies (**Fig 3**A). These bacterial populations appeared to evolve the expected (strongly selected) phenotype of inhibition of flagellar synthesis and/or rotation when passaged in an environment alongside phage χ; the flagellotropic phage is unable to bind and infect host cells that lack functional flagella[19,20]. In contrast, this phenotypic change in cell motility was not observed in the four Control lineages (data not shown).

To probe the genetic basis of motility loss, we sequenced the population genomes of each Treatment lineage at passage 3 and analyzed the data with Breseq[25]. Six of these lineages consisted of nonmotile χ-resistant bacteria ('spotty' colony morphologies), and we focused on these representative consensus genomes. We discovered that an insertion sequence element, IS1, mediated the disruption of motility-related genes. In the ancestral strain MG1655, this transposon-like element is located upstream of *flhDC*, which encodes the master operon of flagellar synthesis, motility, and chemotaxis[11]. Transcription and translation of *flhDC* is essential for the downstream expression of flagellar synthesis, motility, and chemotaxis genes[26]. Analyzing the sequences through Breseq[25], we interpreted the sequencing data in the following manner: in presence of phage χ, the evolving bacterial populations were enriched for mutants where IS1 jumped downstream of *flhD* into various gene locations, thus disrupting the expression of FlhDC (**Fig 3**B,C; n = 6 sequenced populations).

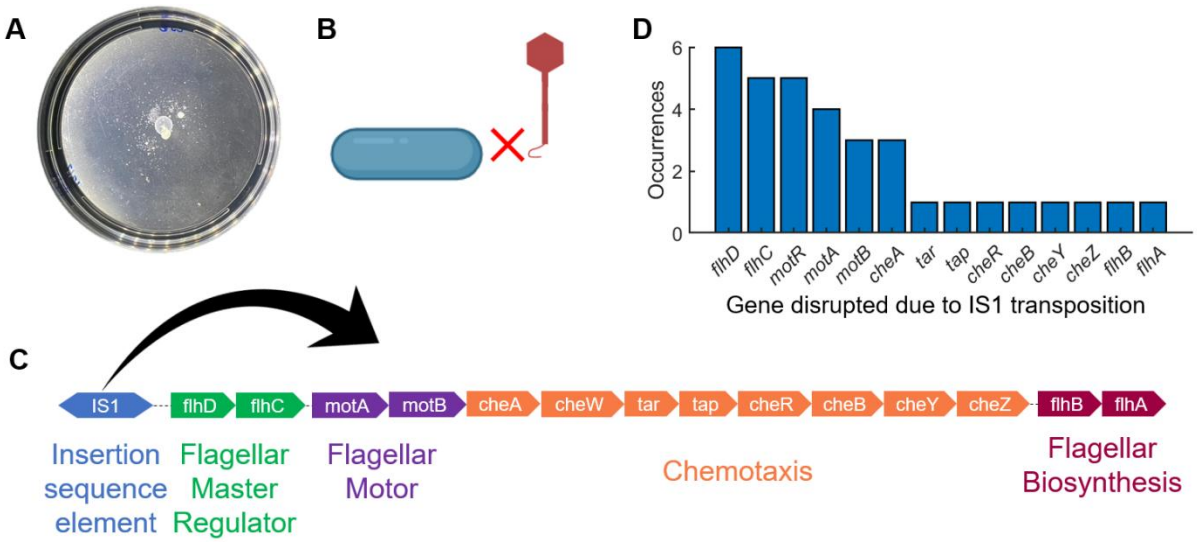

Fig 3. Early in evolution, selection tended to favor χ-resistant mutants that were non-motile. (A) Early in experimental evolution (up to passages 2 and 3), Treatment bacteria developed resistance to phage χ by abolishing flagellar synthesis, as the virus cannot infect bacteria lacking functional flagella **(B)**. The populations did not present visible swim rings and instead showed 'spotty' colonies of bacteria. **(C)** The motility-related mutations were mediated by transposition of insertion sequence element IS1, which is typically upstream of the flagellar regulatory genes. Transposition of IS1 disrupted the expression of FlhDC, the flagellar master operon. The genomes of six representative nonmotile mutant populations were sequenced, and the overall frequency of observed disrupted genes was determined based on the destination of IS1 transposition **(D)**.

Bacteria recover motility later in experimental evolution

Later in the evolution experiment (by passages 3 or 4), visible swim rings were observed on all Treatment-population plates (**Fig 4**A), indicating that motile, phage-resistant variants had emerged. Interestingly, lineage T10 did not show such growth at passage 10, possibly due to phage-driven extinction of host bacteria (**Fig S1**). To determine the genetic changes in these Treatment populations, we obtained consensus whole-genome sequences from each Treatment lineage at passages 5 and 10, and compared these data to the ancestral (reference) genome[25]. Genes with polymorphic sites which are over 10% different than the ancestor sequence are listed in **Table S1** (passage 5) and **Table S2** (passage 10). Notably, several of these genes are involved in chemotaxis, the synthesis of flagellar machinery, or the regulation of flagellar motility. Mutations that occurred at frequencies >70% are shown in **Fig S2**. A large number of high-frequency mutations were found in *fliC*, the gene encoding the flagellin protein, which forms the flagellar filament monomer (**Fig 4**B, **Fig S2**). FliC consists of conserved N- and C-terminal D0 and D1 domains and variable central domains D2 and D3.

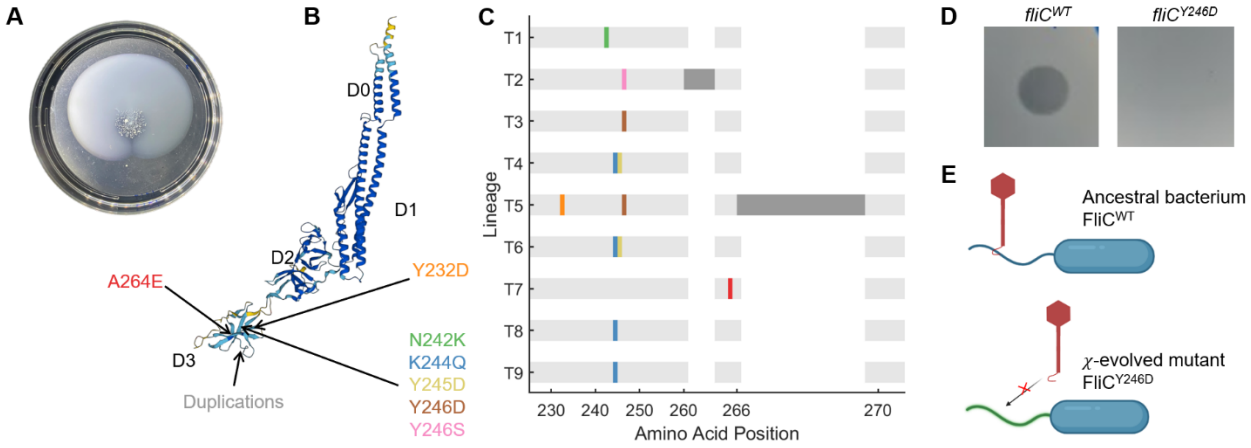

Fig 4. Motile, χ-resistant bacteria feature mutations in the flagellar filament. (A) All treatment populations showed visible swim rings after passage 4. **(B)** Structure of *E. coli* FliC (UniProt P04949) is shown with domains D0, D1, D2, and D3. All observed *fliC* mutations mapped to the D3 domain. **(C)** Amino acid substitutions in FliC are indicated for each endpoint lineage, with the color code described at the bottom. Dark grey corresponds to amino acid sequences that were duplicated (7 AA duplication staring at T260 in T2; 19 AA duplication starting at A266 in T5). **(D)** Phage χ forms characteristic clearing on lawns of the ancestor, while cells carrying the single amino acid substitution Y246D in FliC are resistant to χ. **(E)** These results suggest a mechanism in which targeted mutations in *fliC* prevent χ from binding to the flagellum, allowing cells to evade infection.

We isolated multiple representative mutants (clones) from each endpoint (passage 10) Treatment lineage (at least two and up to seven clones isolated from each lineage) and performed Sanger sequencing of the *fliC* locus. All clones isolated from a single lineage carried identical mutations, so we report the consensus for each Treatment lineage (**Fig 4**B, C). Control lineages did not carry any mutations in *fliC*. Most mutations in the Treatment lineages were single or dual amino acid (AA) substitutions localized to the D3 domain of the flagellin monomer, which remains exposed on the outer surface of the flagellar filament after polymerization[27]. Given the appreciable impact of point mutations on flagellar function[28], we hypothesized that a single amino acid substitution might confer resistance to phage χ. To test this idea, we knocked out the *fliC* gene and complemented the resulting strain with wild-type (ancestor) FliC (as control) or the Y246D variant (**Fig 3**C) (observed in multiple χ-resistant mutants) cloned into the expression vector pTrc99A. When we spotted dilutions of a phage χ lysate onto lawns of these test strains, we observed that clear plaques formed only on the wild-type complement (**Fig 4**D), indicating that Y246D-expressing cells escaped infection. We also constructed a strain via allelic exchange carrying the FliC^{Y246D} point mutant in its native chromosomal locus. The resulting mutant strain

formed swim rings on TB soft agar that were about 90% of those formed by wild-type and exhibited phage resistance. These results suggested that a single AA substitution in the flagellin's D3 domain obstructs the binding of χ, rendering the bacteria resistant to the phage (**Fig 4**E).

Phage χ-resistance trades off and trades up with bacterial motility in soft agar

Two traits under selection can evolve via trade-offs (one trait improves at the other's expense), trade-ups (both traits improve), or may have neither relationship[29,30]. Since χ exploits the flagellar motility apparatus for binding, and motile and resistant cells carried mutations in the flagellar filament, we examined whether motility trades up or trades off with the evolution of χ-resistance in the nine motile endpoint Treatment lineages. Swim-ring diameters after 15 hours were compared to those of the ancestor and Controls, which were serially passaged on swim plates in the absence of phage selection. For each Treatment lineage, we experimented with each clone (isolated from passage 10 of each lineage) in duplicate. We found that the Control lineages did not show statistically significant differences in swim-ring diameter relative to the ancestor. Contrarily, most χ-resistant Treatment lineages (T1-T6) showed swim-ring diameters less than that of the ancestor, indicating an evolutionary trade-off: increased phage-resistance at the expense of decreased motility in soft agar (**Fig 5**A). Lineage T7 showed a swim-ring diameter comparable to that for the ancestor and the evolved Control strains. However, evolved motile lineages T8 and T9 exhibited significantly larger swim rings than the ancestor, with T9 showing significantly greater diameters than the Control isolates C1-C4, demonstrating a trade-up: increased phage-resistance alongside increased motility on soft agar (**Fig 5**A).

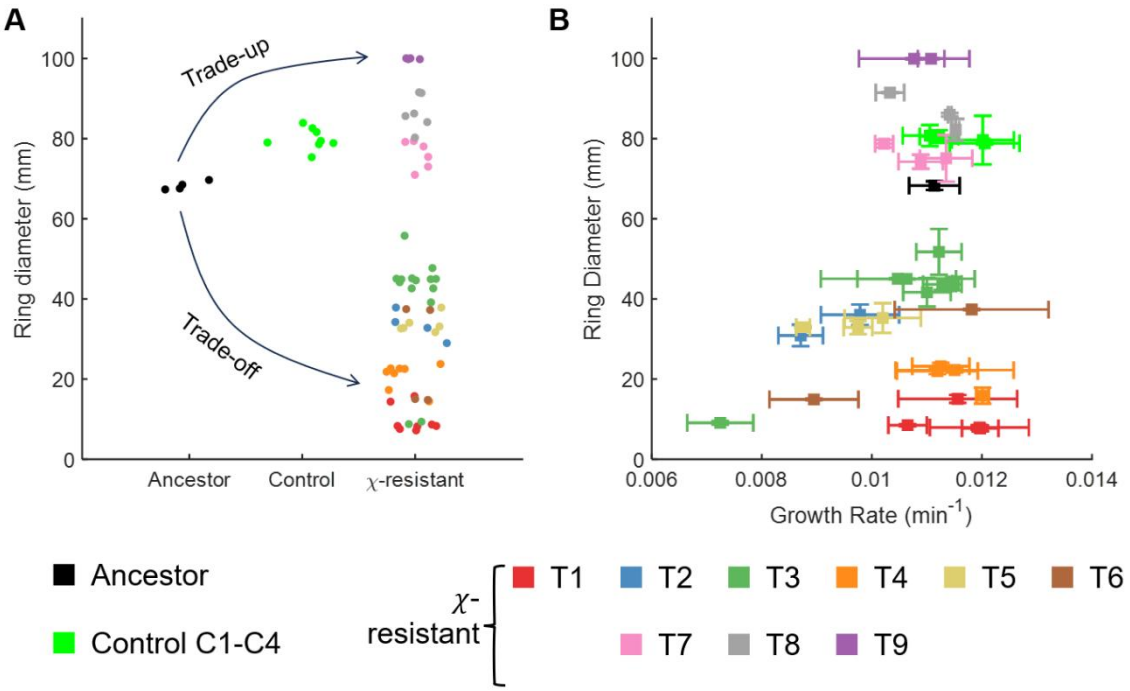

Fig 5. Resistance to phage χ trades off as well as trades up with motility. (A) Swim-ring diameters observed for the ancestor (black), strains isolated from evolved Controls (phage free; bright green), and motile χ-resistant Treatment (phage selection) lineages (color-coded according to Treatment population). Swim-plate assays were conducted in absence of phage χ. Most treatment populations showed evidence of either a motility trade-off with increased phage-resistance, or a motility trade-up with greater phage-resistance (trend indicated by arrows). **(B)** Growth rate of each bacterial strain was measured in well-mixed liquid (on a microplate reader) and plotted against the swim-ring diameter. These observations were uncorrelated (Pearson correlation coefficient, ρ = 0.22, P-value = 0.2). Data points are color-coded based on the Treatment lineage for isolation. For each lineage, at least two (e.g., T6, T9) and at most seven (T3) clones were isolated. All experiments were carried out in duplicate for each clone. Further statistical tests are reported in **Fig S3**.

In an expanding ring of motile bacteria on soft-agar plates, growth (cell division), flagellar motility, and chemotaxis influence the expansion speed[11,31–34]. Recent studies have shown that population growth rates greatly affect expansion speeds[11,35,36]. To test whether the observed differences in swim-ring diameter can be attributed to varying growth rates, we measured the growth rates of the isolated endpoint clones (passage 10) using an automated spectrophotometer (microplate reader) where light scattering provides a proxy for cell density. We plotted the swim-ring diameter of each strain or clone against its growth rate estimate (**Fig 5**B). These measured quantities showed no significant correlation (Pearson correlation coefficient ρ = 0.22, P = 0.2), suggesting that differential growth rate is not the primary factor influencing swim-ring diameter of

the isolated treatment clones. Instead, mutations in the flagellar filament (**Fig 4**) and other related genes (such as genes encoding components of the flagellar motor or the chemotaxis pathway which is an upstream controller of flagellar motility, **Fig S2**) likely alter the chemotaxis-ability (measured as the 'chemotactic coefficient'[11,31–34]) of the evolved Treatment strains in nutrient soft agar[37].

χ-resistance alters single-cell distributions of motility traits

After ruling out a general growth effect, we hypothesized that differences in chemotactic efficiency and/or motility may account for the observed variations in swim-ring diameters. To test this idea, we quantified single-cell swimming behavior through phase-contrast microscopy and single-particle tracking. We performed these experiments for the ancestral and evolved strains with a single representative clone isolated from each end-point (passage 10) Treatment and Control lineage, as the flagellar mutations observed across all strains in each Treatment lineage were identical (**Fig 4**C). We observed that a majority of cells in some of these clonal populations were non-motile, and hence calculated the fraction of motile cells for each of the experimental lineages (**Fig 6**A). These data suggested that motile cells formed the swim rings on assay plates, whereas in some lineages the majority fraction of non-motile cells remained closer to the center of the plate. We observed that clones isolated from Treatment populations with reduced swim-ring diameters (lineages T1-T6) had significantly lower motile fractions than the ancestor. In contrast, the motile fraction in the remaining Treatment lineages (T7-T9) was comparable to the ancestor and the Control lineages (**Fig 6**A). We confirmed for each representative clone that motile cells remained fully resistant to phage χ (**Fig S4**). Next, for each motile subpopulation we calculated the distributions of swimming speed (**Fig 6**B). All clones from Treatment and Control lineages, except from lineage T7, had significantly different swimming speed distributions relative to the ancestor (**Fig 6**B). We also determined the tumble bias – the fraction of time that the cells spend tumbling (**Fig 6**C). All clones from Treatment lineages, except from T7, displayed a higher tumble bias relative to the ancestor, while 3 of 4 Control lineages displayed a tumble bias lower than the ancestor (**Fig 6**C).

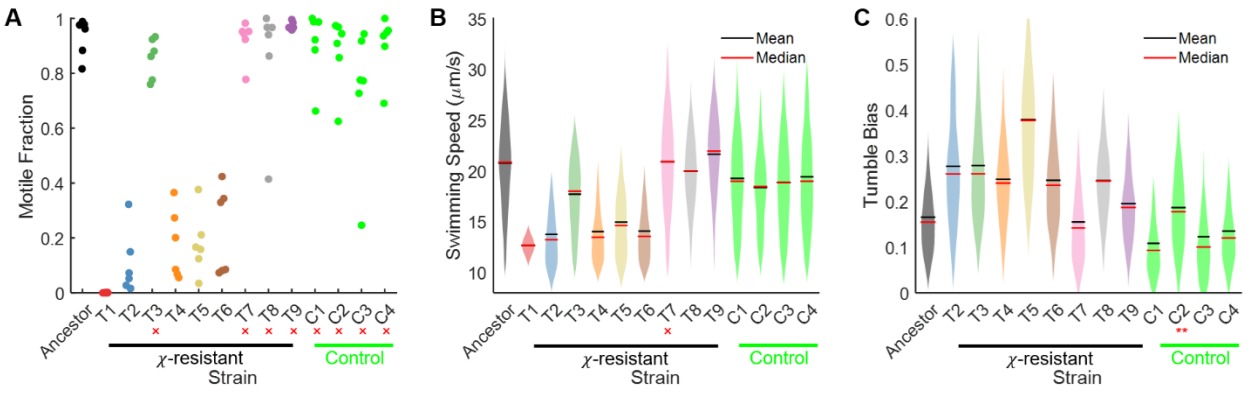

Fig 6. Motile fraction, swimming speed, and tumble bias of evolved strains often differ from traits of the ancestor. Single-cell motility was recorded with phase-contrast microscopy and analyzed using automated algorithms. **(A)** Motile fraction was calculated for a representative strain from each evolved lineage. **(B)** Distributions of single-cell swimming speeds are shown for each strain. **(C)** Tumble bias distributions of single cells are indicated for each strain (except χ-resistant strain T1, which was essentially non-motile). ANOVA yielded $P < 10^{-4}$ for each dataset. Post-hoc Dunnett's multiple comparisons tests were performed to compare each evolved strain with the ancestor. Strains marked with a red cross (×) showed no significant difference from the ancestor, while all the other observations differed significantly from the ancestor: $P < 10^{-4}$ for all observations (not indicated) except tumble bias distribution for strain C2 which had $P < 0.01$, indicated with **).

χ-resistant mutants have altered chemotaxis kinase activity

We expected the flagellar mutations to modulate motile fraction and swimming speeds, because change in flagellar structure (through AA substitutions characterized in **Fig 4**) may modulate the function. However, the change in tumble bias was somewhat surprising, as it is reflective of the chemotaxis response in wild-type cells, although it cannot be ruled out that mutant flagellar filaments cause the formation of an altered flagellar bundle, which could affect bias behavior. To evaluate the chemotaxis response of evolved isolates independent of flagellar filament function, we used a Förster Resonance Energy Transfer (FRET)-based approach to measure chemotaxis kinase activity in the ancestor strain and the evolved isolates[21,22]. In this assay, the addition and removal of a saturating concentration of the non-metabolizable chemoattractant α-methyl-aspartate (MeAsp) allows the determination of the chemotaxis kinase activity. An exemplary trace of the kinase activity is shown in **Fig 7A**: upon addition (removal) of the attractant, the kinase activity goes down (up) and 'adapts' back to the basal value over time[21,22]. From the trace, we calculated three parameters of the kinase response: basal activity (a_0), rate of adaptation (r), and precision in adaptation (a_{adap}/a_0), since adaptation to stimulus addition is typically imperfect for large ligand concentrations[38]. We measured chemotaxis kinase

activity for the ancestor and three representative evolved bacterial strains: one clone isolated from an evolved trade-off lineage, T5, for which resistance to χ coincided with decreased motility, and two clones isolated from evolved trade-up lineages, T8 and T9, for which χ-resistance coincided with increased motility. Parameters of the kinase responses for each strain are indicated in **Fig 7B, C , D**. The basal activity of the chemotaxis kinase appeared to be elevated in all evolved strains as compared to the ancestor, and this elevation was statistically significant for T5 (**Fig 7B**). Trade-up strains T8 and T9 showed statistically significantly faster kinase adaptation as compared to the ancestor, while trade-off strain T5 was comparable to the ancestor (**Fig 7C**). The adaptation was more precise in the trade-up strain T8 (and showed an upward trend in T9), while the trade-off strain T5 adapted less precisely as compared to the ancestor (**Fig 7D**). Overall, we observed that the motility-trade-up strains T8 and T9 evolved to adapt faster and more precisely, while the trade-off strain T5 did not.

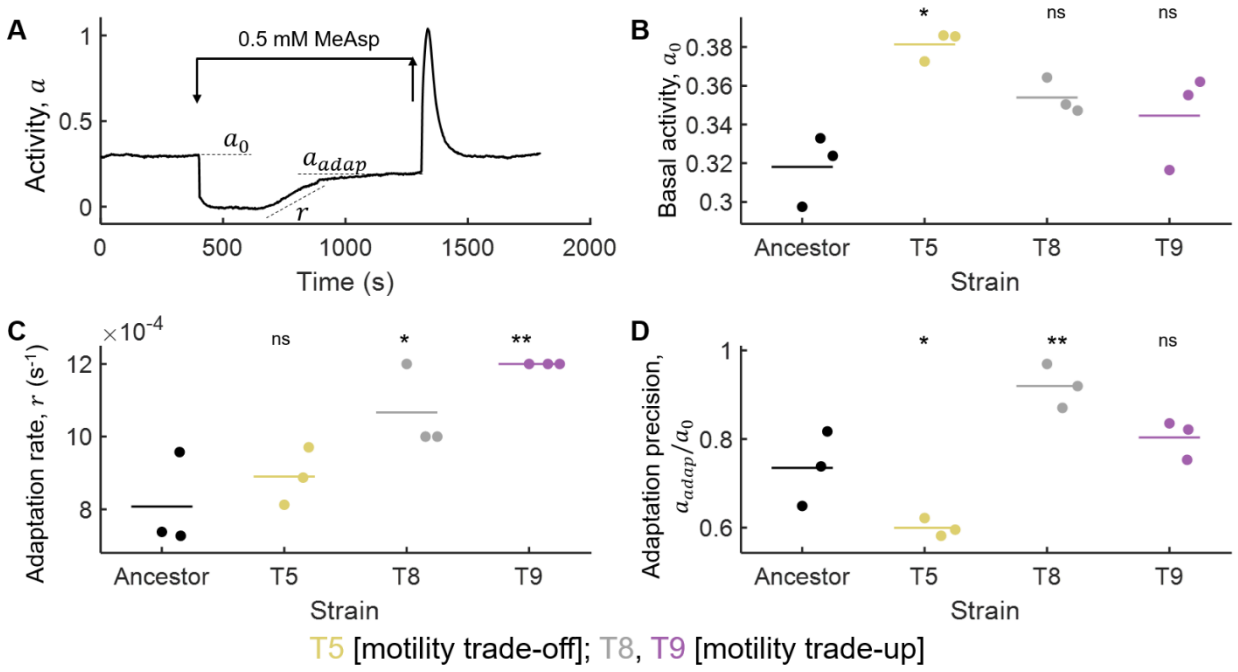

Fig 7. Evolved strains respond differently to chemotactic stimuli. (A) An example trace of the kinase activity (ratiometric FRET between CheZ-RFP and CheY-YFP) is shown. The arrows indicate the time when a saturating concentration of chemoattractant methyl-aspartate (0.5 mM) was flowed into and out of the sample chamber. Basal activity a_0, adapted value of activity a_{adap}, and adaptation rate r are indicated with dashed lines (r is calculated as the slope of the line, whereas a_0 and a_{adap} are Y-values). Each trace is an output from observations of hundreds of cells within the microscopic region of interest. Basal activity a_0 **(B)**, adaptation rate r **(C)**, and adaptation precision calculated as the ratio of the adapted and basal values of kinase activity, a_{adap}/a_0 **(D)** for three independent replicated experiments are indicated as dots for each

strain. Mean values are indicated as dashes. For each parameter in **B-D**, ANOVA yielded $P < 0.01$ for each dataset. Post-hoc Dunnett's multiple comparisons tests were performed to compare each representative lineage strain with the ancestor (* $P < 0.05$, ** $P < 0.01$, ^{ns} no significant difference from the Ancestor group).

Discussion

Flagellotropic phages are commonly found in natural samples and may have existed alongside bacteria for billions of years of evolution[5,14,39–44]. Motile bacteria may regularly encounter flagellotropic phages, yet the evolutionary mechanisms of bacterial resistance to these phages are rarely studied[12]. We examined the genetic and phenotypic consequences for bacteria when they evolve in microcosms that allow cell motility and contain flagellotropic phage predators, using the model system bacterium *E. coli* and phage χ. Instead of using well-mixed environments (e.g., shaking culture-flasks) typical of many phage-bacteria coevolution experiments, we challenged bacteria to evolve in spatially confined swim plates, to constrain motility while applying selection pressure from phage χ. This design selected for χ-resistant bacteria and the possibility for motility maintenance.

Phage χ is known to infect both *E. coli* and *Salmonella enterica*[19,45], which possess a similar motility and chemotaxis machinery[16]. In *E. coli*, results from our evolution experiment show that all mutations that disrupt χ infection are in the outermost D3 domain of *E. coli* flagellin (**Fig 4**B). A targeted domain deletion and swapping approach in *S. enterica* revealed that the N- and C-terminal D2 domains are the major determinants of phage susceptibility and that the D3 domain plays a less-crucial role [46]. These two results appeared to be in some disagreement. However, we also discovered that most of the Treatment lineages had an increased tumble bias (**Fig 6**C). In addition, all FliC point mutations that resulted in phage resistance experienced a charge change in the amino acid side chain. The altered charge may have varied the orientation of loops resulting in altered flagellar bundle formation, as well as modified the overall epitope needed for χ to bind. In addition to the mutations in flagellar motor and chemotaxis machinery (**Fig 4**, **Table S1, Table S2**), some of our populations also acquired mutations in genes involved in the synthesis or regulation of outer-surface structures such as lipopolysaccharides (LPS) and capsules. For instance, one Treatment lineage presented a majority (>70% frequency) of genotypes with a mutation in the LPS-biosynthesis gene *waaQ* at passages 5 and 10 (**Fig S2**). The gene encoding phosphotranferase RcsD (involved in capsular polysaccharide synthesis) also showed presence of a mutation at >70% frequency at passage 10 in one lineage (**Fig S2**). LPS-related genes were similarly observed in an earlier study that imposed phage χ selection pressure on *E. coli*[47]. Additionally, flagellotropic phage 7-7-1 uses LPS as the secondary receptor to infect its

host *Agrobacterium* sp.[40]. Model coliphage T4 also uses LPS as a co-receptor[48,49]. On the other hand, several mutations in LPS biosynthesis and Rcs pathways are known to have pleiotropic effects in reducing motility[50,51]. Our results suggest two possibilities: either that phage χ may use LPS in some capacity during the cell adsorption and genome injection processes, or, more likely, that reduced motility in the LPS biosynthesis and Rcs mutants may provide limited resistance against χ.

After initially attaching to *Salmonella enterica* serovar Typhimurium 14028 via binding to the flagellum, χ may use the AcrABZ-TolC multidrug efflux pump as a receptor to inject its genome, as deletions in individual genes encoding the system drastically reduced infection[45]. One of the important functions of efflux pumps is the active removal of certain antibiotics if they enter the cell. Phages that bind to efflux pumps of host bacteria represent interesting candidates for phage therapy development because evolved phage-resistance may occur through altered or deleted efflux pump proteins, thus potentially re-sensitizing bacteria to certain chemical antibiotics[1,52]. Interestingly, we did not observe any mutations in the genes encoding these efflux pump proteins in our *E. coli* Treatment lineages with evolved resistance against χ. It is possible that phage χ uses the efflux pump protein complex to inject its genome in *E. coli*, but the binding-related mutations in the flagellum were sufficient to resist χ-attack. To test this hypothesis, we used a *tolC* knockout and tested if cells of this strain can swim through concentrated spots of phage χ on swim plates. We observed that while cells of our Δ*tolC* mutant moved slower than the wild-type, they were still susceptible to χ infection (**Fig S5**). Thus, we did not find strong evidence for involvement of the TolC efflux pump in the evolution of *E. coli* resistance to χ infection in our study.

Antibiotic-resistant bacteria often carry mutations in 16S and 23S rRNA genes, as antibiotics commonly target these ribosomal RNA components. Recent evidence suggests that phage-resistance may also induce mutations in these regulatory genomic regions[53]. We observed mutations in the genes encoding 16S and 23S rRNA regions of several χ-resistant mutants (**Fig S2**). This finding suggests that phage-resistance may also influence the effects of certain antibiotics on cells.

In the current model of χ-attachment to the flagellum, counterclockwise rotation of the flagellum (as viewed from the distal end), drives the phage towards the cell body[19]. In this model, clockwise rotation of the flagellum would propel the phage away from the cell. The run-tumble motion of *E. coli* cells results from switching between counterclockwise and clockwise flagellar rotation, which causes runs and tumbles, respectively[16]. *E. coli* cells predominantly rotate counter-

clockwise, resulting in more runs than tumbles[8,16]. Therefore, χ infection utilizes the more frequent counterclockwise direction of flagellar rotation. Our kinase activity measurements revealed higher mean kinase activity in the evolved lineages (**Fig 7**B: statistically significant difference in mean a0 for trade-off strain T5, with upward trends for T8 and T9). Higher kinase activity increases phosphorylation of CheY, where CheY-P promotes clockwise rotation of flagellar motors. Additionally, our single-cell tracking experiments showed that tumble bias increased in most evolved, χ-resistant lineages. This increased tumbling may result from either a higher fraction of clockwise (tumble-inducing) flagellar rotation or altered bundle stability due to amino acid substitutions in FliC. Together, these experiments suggest that higher tumbling and possibly increased clockwise rotation evolved in our lineages, though the latter would require direct measurement of single flagellar motor rotation to confirm[8]. We do not believe our results indicate adaptive changes in tumbling specifically to resist χ attack; rather, we propose that amino acid substitutions in FliC confer resistance to χ, while elevated tumble bias may be a secondary phenotype that reduces the probability of χ reaching the cell body.

E. coli has served as a model system for studying bacterial motility and chemotaxis[16]. Activity of the chemotaxis kinase CheA can be measured using a FRET-based approach[21,22]. Recent work has shown remodeling in motility as well as the chemotaxis network and specifically CheA activity, during evolution of motile *E. coli* on swim-plates[34,54]. Response of CheA activity to α-methyl-aspartate, a strong chemoattractant known to trigger a response in the chemotaxis network, is well-characterized[22,55]. The Treatment strain T5 that evolved a tradeoff between decreased motility and increased χ-resistance showed an elevated basal CheA activity and adapted less precisely as compared to the ancestor. In contrast, the evolved Treatment strains T8 and T9 that presented trade-ups (increases in both motility and χ-resistance), likely recovered their performance by evolving faster and more precise adaptation (**Fig 7**). The fact that the trade-up strains adapt faster than the ancestor likely explains how these strains expand faster without having a significantly higher swimming speed or growth rate[38]. Albeit, we do not believe that the AA substitutions in the FliC are responsible for the changes in CheA response; rather, other mutations within chemotaxis and motility genes (**Table S1, Table S2**) likely modulated the kinase response. Future experiments using recombinant genetics could resolve which specific mutation(s) were responsible for the observed changes in kinase activity. We believe this is the first evidence of evolutionary pressure from a phage remodeling the dynamics of regulatory pathways (chemotaxis signaling in this case) upstream of the phage receptor (flagella in this case).

The century-old approach of using phages as therapeutics is experiencing resurged interest due to the alarming rise in antibiotic-resistant bacterial infections[4]. Evolutionary trade-offs can be leveraged in phage therapy, such that target bacteria are killed while therapeutic phages select for mutants that resist phage attack alongside phenotypic changes that reduce pathogenicity[1]. However, trade-ups may also occur, potentially making the target bacteria resist phage infection while becoming more pathogenic[29]. Because motility is a fitness or virulence factor in many bacterial species[13], flagellotropic phages offer exciting therapeutic options[5]. Our results demonstrate that *E. coli* cells exposed to phage χ first evolve resistance by forfeiting motility, implying a potentially advantageous fitness and/or virulence trade-off. In a clinical setting, the remaining non-motile bacteria would be less capable of host colonization and could be more readily eliminated by immune defenses or co-therapy with antibiotics. Thus, the early stages of 'flagellotropic-phage-steered' bacterial evolution are relevant in therapy development, while caution is needed when considering later stages of evolution due to the possibilities for trade-ups.

According to later stages of our experiments, persistent phage selection may favor χ-resistant cells that preserve motility. This perhaps represents ecological settings in which bacteria may encounter an environment perpetually rich in phages. To survive and potentially escape phage attack in such an environment, bacteria would be advantaged by evolving resistance to flagellotropic phages while simultaneously retaining motility. In our model system of *E. coli* and χ phage, this balance was achieved through mutations in the flagellar filament that preclude χ-binding without disabling swimming. Thus, our results suggest that the evolutionary response of bacteria to flagellotropic phages is not straightforward and may depend on the duration of phage selection in addition to random mutational variation across populations.

Materials and Methods

Bacteria and phage strains

MG1655 was used as the wild-type (WT) *E. coli* ancestor strain, which was obtained from J. Wertz at the Coli Genetic Stock Center (CGSC) at Yale University, now re-branded as *E. coli* Genetic Resource Center (https://ecgrc.net/). *Salmonella*-infecting χ-phage was obtained from Kelly Hughes at the University of Utah and grown on the permissive (Δ*recA*) strain BW25113 to change its methylation signature to *E. coli*.

The Δ*fliC* mutant of MG1655 was generated through P1-transduction, replacing the *fliC* gene with a Kanamycin resistance cassette. The Y246D amino acid substitution ($fliC^{Y246D}$) was made on the isolated *fliC* gene via site-directed mutagenesis by substituting T at nucleotide

position 736 with a G. The unmodified (*fliC*^{WT}) or modified (*fliC*^{Y246D}) flagellin was then cloned into plasmid vector pTrc99A using XbaI and SalI restriction enzymes. Supplemental 100 µg/mL ampicillin and 20 µM IPTG were added to the cultures and plates when growing these strains.

The chromosomal mutant of MG1655 carrying FliCY246D was constructed using allelic exchange with the suicide vector pWM91and the diamino pimelic acid auxotrophic, conjugative *E. coli* strain B2155[56]. The mutant was confirmed by PCR and Sanger sequencing.

Culture conditions

Tryptone Broth (TB; 10 g tryptone, 5 g NaCl per L) was used for liquid cultures, 1.5% agar plates, 0.5% top agar for the double-layer method of phage propagation and 0.3% swim agar for swim plate assays. Overnight cultures were initiated from colonies grown on solid (1.5%) TB agar and placed into TB liquid medium, incubated with shaking (150 RPM) at 30°C. Bacterial stocks were stored in 25% glycerol at -80°C. High-titer stocks (lysates) of phages were grown by mixing a virus with its wild-type host bacteria in liquid broth and incubating for 12-24 hours as described above to allow phage population growth, followed by centrifugation and filtration (0.22 µm) to remove bacteria and obtain a cell-free lysate. Phages were enumerated (plaque-forming units [PFU] per mL) using the standard double-layer agar method where viruses form visible plaques on confluent lawns of wild-type host bacteria within 0.5% top agar, overlayed on 1.5% agar in the bottom layer.

Evolution Experiment

Treatment lineages of *E. coli* were passaged as follows. Soft-agar swim plates (Tryptone Broth [TB] with 0.3% agar) were embedded with a high concentration of χ-phage to ensure that bacteria frequently encounter phages while swimming: 15 µL of 10^{11} PFU/mL χ-phage were added to 10 mL of agar in each plate. This concentration of phages was determined by carrying out a preliminary experiment to test the lowest phage concentration that suppressed bacterial swim ring formation for 24 h. For the evolution experiment, a phage titer 10-fold greater than the threshold was used. Five microliter of overnight culture of MG1655 (the ancestral strain) grown in TB was inoculated in the center of the plates followed by incubation for 24-48 h at 30°C.

After each passage (until swim rings appeared or 48 hours elapsed), plates were processed as follows: the contents of the plate were pooled into a tube with 10 mL TB and homogenized by vortexing. Next, 10 µL of the mixture (effectively 5 µL of the previous plate's contents) was inoculated into a fresh swim plate containing phage χ at the same concentration as indicated above (1:2000 bottleneck). Plates were incubated at 30°C and a frozen stock in 25%

glycerol was made from the remaining mixture. This process was repeated for 10 passages, with 10 independent replicates all initiated from the same MG1655 ancestor genotype (**Fig 2**). Each new passage occurred after 24 hours if a motile ring of bacteria was observed. If no motile ring was present (which was the case for the first 2-3 passages), incubation continued until 48 hours. This method allowed us to determine if the χ-resistant bacteria growing on the plate remained motile. Four Control populations of *E. coli* were passaged identically, in the absence of phage.

Isolation of bacteria from evolution experiment

At least two individual isolates (clones) were obtained from each Treatment and Control lineage at passage 10. The frozen stock was streaked on 1.5% TB agar plates to obtain isolated colonies. Individual isolated colonies were picked and re-streaked onto fresh plates. Individual colonies from the second (doubly-isolated) plate were used for experiments with the isolates (**Fig 4**, **Fig 5**).

Sequencing and mutant calling analysis

For whole genome sequencing of each Treatment lineage at passages 5 and 10, 200 µL of frozen stock were placed in 5 mL TB and incubated overnight at 30°C. After incubation, 1 mL of each culture was pelleted by centrifugation and sent to SeqCenter, where genomic DNA was extracted and libraries were prepared for Illumina sequencing (paired-end reads of 151 bp length collected to a final coverage of ~100-fold across the reference genome). Mutant calling analysis was performed using Breseq with default mode[25].

Bacterial growth rate measurements

Isolates were grown overnight in TB medium at 30°C, then diluted 1:200 into 200 µL fresh TB. Each isolate was assayed in triplicate with their positions on the 96-well plate randomized using the *PlateDesigner* application[57]. Cultures were incubated at 30°C with shaking, and optical density at 600 nm was monitored at 10-min intervals for 24 h by a BioTek Synergy H1 microplate reader. The growth rate was calculated by obtaining an exponential fit for the OD_{600} values over time for each strain in the area of the growth where $\log(OD_{600})$ versus time is linear.

Single-cell tracking experiments

Overnight cultures were grown at 30°C in TB medium, diluted 1:100 in fresh TB, and re-grown for 4 hours at 30°C, reaching the exponential phase of growth (OD_{600} ~ 0.4-0.5). Exponential-phase cells were diluted into Motility Buffer (MB: 0.01 M potassium phosphate, 0.067 M NaCl, 0.1 mM EDTA, 1 µM methionine, 10 mM lactic acid, pH 7.0) to an OD_{600} ~ 10^{-4} and allowed to equilibrate (chemotactically adapt to MB) at room temperature for 20 min before

experiments were performed. Cells were then introduced to an imaging chamber made by affixing #1.5 coverslips to glass slides via double-sided sticky tape. Both glass slides and coverslips were freshly cleaned (on the same day) with vacuum gas plasma to make their surfaces hydrophilic, thereby preventing adhesion of cells to these surfaces. After introducing the sample, the chamber was sealed on both sides with VALAP (equal parts Vaseline®, lanolin, and paraffin wax) to prevent fluid flow. Swimming cells were visualized at 30°C with a Nikon Ti-E inverted microscope using a CFI Plan Fluor 4X/0.13 NA objective and PhL ring for phase-contrast. Movies were recorded at 20 frames per second and analyzed in MATLAB using an algorithm described previously[33,55].

Calculation of motile fraction, swimming speed, and tumble bias

Distributions of the swimming speed featured a peak ~ 5 μm/s. Control experiments with the non-motile MG1655 Δ*fliC* strain confirmed the peak to be due to non-motile cells (**Fig S6**). Because this peak terminated at 8-10 μm/s, cells with speeds < 10 μm/s were classified as non-motile. Therefore, the motile fraction in each experiment was defined as the portion of trajectories exceeding the 10 μm/s threshold.

Swimming speed and tumble bias were calculated as described previously[33,55]. Briefly, a custom MATLAB algorithm was used to categorize trajectory segments as 'run' or 'tumble'. Tumbles were primarily identified using angular speed: local minima and maxima were defined, and a tumble was identified if the total angular change over a local angular velocity peak exceeded a threshold of $4\sqrt{D_r \Delta t}$ (rotational diffusion constant assumed as $D_r = 0.1\, rad^2/s$). The tumble duration was defined as the interval where the angular speed remained above 50% of the peak value, provided it did not drop below an exit threshold of $15\, rad/s$. Additionally, linear speed criteria were employed to identify tumbles. A speed-based tumble was called if the depth of a local speed minimum (Δv, relative to adjacent maxima) was at least 2.5 times the minimum speed. For these events, the tumble was defined as the period where the speed remained within 25% of the minimum value relative to the recovery. Finally, any single-frame gaps between detected tumbles were filled to account for temporal down-sampling. For each trajectory, the mean swimming speed was calculated as the average translational speed during non-tumble periods, and the tumble bias was calculated as the ratio of time spent tumbling to the total trajectory time.

In vivo FRET microscopy

Cells were transformed with plasmid pSJAB106, which expresses CheZ–YFP and CheY–mRFP1 fusion proteins in tandem (constituting a FRET pair) under IPTG induction, and contains an ampicillin-resistance cassette for selection[22]. Cells were grown overnight at 30°C in TB,

549 supplemented with 100 μg/mL ampicillin to ensure plasmid retention. Overnight cultures were
550 then diluted 1:50 into 10 mL of fresh TB supplemented with 50 μM IPTG and 100 μg/mL ampicillin
551 and then grown at 30°C until they reached an OD_{600} of 0.45-0.46. Cells were subsequently
552 washed twice with MB^- (Motility Buffer described above, without NaCl) and resuspended in 2 mL
553 MB^-. The suspension was incubated at room temperature for 90 min to allow fluorophore
554 maturation.

555 For FRET imaging, 60 μL of cell suspension were incubated on a coverslip coated with
556 poly-L-lysine (Sigma) for 10 min to attach cells, then transferred to a flow cell under continuous
557 flow of MB^- (400 μL/min) maintained by a syringe pump (PHD 2000, Harvard Apparatus).
558 Solutions in MB^- were used to add and remove 500 μM α-methyl-aspartate (MeAsp; Sigma).

559 FRET imaging was performed on an inverted microscope (Eclipse Ti-E, Nikon) equipped
560 with a 60× oil-immersion objective (CFI Apo TIRF, Nikon). YFP excitation took place every 2 s
561 using a broad-spectrum LED (SOLA SE, Lumencor) with a pulse duration of 50 ms. Excitation
562 light was passed through two excitation filters (59026x, Chroma; FF01-500/24-25, Semrock) and
563 a dichroic mirror (FF520-Di02, Semrock). Emitted light was split into two channels using an image
564 splitter (OptoSplit II, Cairn Research) equipped with a dichroic mirror (FF580-FDi01-25×36,
565 Semrock) and two emission filters (FF01-542/27 and FF02-641/75, Semrock), projecting YFP and
566 RFP signals side-by-side onto a single sCMOS camera (ORCA-Flash 4.0 V2, Hamamatsu). A
567 dense monolayer of approximately 500 cells was imaged in each experiment. Images were binned
568 4×4 to maximize signal-to-noise ratio. All experiments were carried out at room temperature
569 (~22°C).

570 To correct for the drift in fluorescence intensities primarily due to fluorophore bleaching,
571 the population FRET ratio (defined as the ratio of the raw emitted RFP and YFP signals) was
572 fitted with a double exponential function. Subsequently, the FRET ratio was divided by the double
573 exponential and normalized between zero (activity upon addition of a saturating dose of 500 μM
574 attractant MeAsp) and one (activity upon attractant removal). Hence, the kinase activity was
575 calculated as:

576

577 $$\mathrm{a} = \frac{FRET(t) - FRET_{saturating}}{FRET_{removal} - FRET_{saturating}}$$

Acknowledgements

We thank Kelly Hughes for gifting us a stock of phage χ, John Wertz for his help in generating the *fliC* knockout for this work, Ece Karatan for plasmid pWM91, and Jun Zhu for *E. coli* B2155. We also thank Turner Lab members including Noah Houpt, Kaitlyn Kortright, Catherine Hernandez, Michael Blazanin, Dallas Mould, Albert Vill, Helen Stone, and others as well as Jeremy Moore, Lam Vo, Jake Sumner, and other members of the Yale Quantitative Biology Institute for interesting discussions and valuable feedback about this work. This study was funded by Yale University through Yale's Center for Phage Biology and Therapy. FA and TE acknowledge support from NIH (R01GM106189-09 and 1R35GM158058-01). JDA and PET acknowledge funding support from Howard Hughes Medical Institute Emerging Pathogens Initiative grant.

References

1. Oromí-Bosch, A., Antani, J. D. & Turner, P. E. Developing Phage Therapy That Overcomes the Evolution of Bacterial Resistance. *Annu. Rev. Virol.* **10**, 503–524 (2023).
2. Koskella, B. & Brockhurst, M. A. Bacteria–phage coevolution as a driver of ecological and evolutionary processes in microbial communities. *Fems Microbiol. Rev.* **38**, 916–931 (2014).
3. Nobrega, F. L. *et al.* Targeting mechanisms of tailed bacteriophages. *Nat. Rev. Microbiol.* **16**, 760–773 (2018).
4. Kortright, K. E., Chan, B. K., Koff, J. L. & Turner, P. E. Phage Therapy: A Renewed Approach to Combat Antibiotic-Resistant Bacteria. *Cell Host Microbe* **25**, 219–232 (2019).
5. Esteves, N. C. & Scharf, B. E. Flagellotropic Bacteriophages: Opportunities and Challenges for Antimicrobial Applications. *Int. J. Mol. Sci.* **23**, 7084 (2022).
6. Kearns, D. B. A field guide to bacterial swarming motility. *Nat. Rev. Microbiol.* **8**, 634–644 (2010).
7. Wong, G. C. L. *et al.* Roadmap on emerging concepts in the physical biology of bacterial biofilms: from surface sensing to community formation. *Phys. Biol.* **18**, 051501 (2021).
8. Antani, J. D. *et al.* Mechanosensitive recruitment of stator units promotes binding of the response regulator CheY-P to the flagellar motor. *Nat. Commun.* **12**, 5442 (2021).
9. Chawla, R., Gupta, R., Lele, T. P. & Lele, P. P. A Skeptic's Guide to Bacterial Mechanosensing. *J. Mol. Biol.* **432**, 523–533 (2020).
10. Colin, R., Ni, B., Laganenka, L. & Sourjik, V. Multiple functions of flagellar motility and chemotaxis in bacterial physiology. *FEMS Microbiol. Rev.* **45**, fuab038 (2021).

11. Cremer, J. *et al.* Chemotaxis as a navigation strategy to boost range expansion. *Nature* **575**, 658–663 (2019).
12. Koskella, B., Taylor, T. B., Bates, J. & Buckling, A. Using experimental evolution to explore natural patterns between bacterial motility and resistance to bacteriophages. *ISME J.* **5**, 1809–1817 (2011).
13. Matilla, M. A. & Krell, T. The effect of bacterial chemotaxis on host infection and pathogenicity. *FEMS Microbiol. Rev.* **42**, fux052 (2018).
14. Gambino, M. & Sørensen, M. C. H. Flagellotropic phages: common yet diverse host interaction strategies. *Curr. Opin. Microbiol.* **78**, 102451 (2024).
15. Sourjik, V. & Wingreen, N. S. Responding to chemical gradients: bacterial chemotaxis. *Curr. Opin. Cell Biol.* **24**, 262–268 (2012).
16. Berg, H. C. *E. Coli in Motion*. (Springer New York, NY, 2004).
17. Wadhwa, N. & Berg, H. C. Bacterial motility: machinery and mechanisms. *Nat. Rev. Microbiol.* **20**, 161–173 (2022).
18. Moore, J. P. & Emonet, T. Physics of bacterial chemotaxis. *Curr. Biol.* **34**, R972–R977 (2024).
19. Samuel, A. D. T. *et al.* Flagellar determinants of bacterial sensitivity to χ-phage. *Proc. Natl. Acad. Sci. U. S. A.* **96**, 9863–9866 (1999).
20. Ravid, S. & Eisenbach, M. Correlation between bacteriophage chi adsorption and mode of flagellar rotation of Escherichia coli chemotaxis mutants. *J. Bacteriol.* **154**, 604–611 (1983).
21. Sourjik, V. & Berg, H. C. Binding of the Escherichia coli response regulator CheY to its target measured in vivo by fluorescence resonance energy transfer. *Proc. Natl. Acad. Sci.* **99**, 12669–12674 (2002).
22. Keegstra, J. M. *et al.* Phenotypic diversity and temporal variability in a bacterial signaling network revealed by single-cell FRET. *eLife* **6**, e27455 (2017).
23. Schavemaker, P. E. & Lynch, M. Flagellar energy costs across the tree of life. *eLife* **11**, e77266 (2022).
24. Keegstra, J. M., Carrara, F. & Stocker, R. The ecological roles of bacterial chemotaxis. *Nat. Rev. Microbiol.* **20**, 491–504 (2022).
25. Deatherage, D. E. & Barrick, J. E. Identification of Mutations in Laboratory-Evolved Microbes from Next-Generation Sequencing Data Using breseq. in *Engineering and Analyzing Multicellular Systems: Methods and Protocols* (eds Sun, L. & Shou, W.) 165–188 (Springer, New York, NY, 2014). doi:10.1007/978-1-4939-0554-6_12.
26. Chevance, F. F. V. & Hughes, K. T. Coordinating assembly of a bacterial macromolecular machine. *Nat. Rev. Microbiol.* **6**, 455–465 (2008).

27. Yonekura, K., Maki-Yonekura, S. & Namba, K. Complete atomic model of the bacterial flagellar filament by electron cryomicroscopy. *Nature* **424**, 643–650 (2003).
28. Alvi, S. *et al.* Flagellar point mutation causes social aggregation in laboratory-adapted Bacillus subtilis under conditions that promote swimming. *J. Bacteriol.* **206**, e00199-24 (2024).
29. Burmeister, A. R. & Turner, P. E. Trading-off and trading-up in the world of bacteria–phage evolution. *Curr. Biol.* **30**, R1120–R1124 (2020).
30. Frank, S. A. *Microbial Life History: The Fundamental Forces of Biological Design*. (Princeton University Press, 2022).
31. Phan, T. V. *et al.* Direct measurement of dynamic attractant gradients reveals breakdown of the Patlak–Keller–Segel chemotaxis model. *Proc. Natl. Acad. Sci.* **121**, e2309251121 (2024).
32. Mattingly, H. H. & Emonet, T. Collective behavior and nongenetic inheritance allow bacterial populations to adapt to changing environments. *Proc. Natl. Acad. Sci.* **119**, e2117377119 (2022).
33. Vo, L. *et al.* Nongenetic adaptation by collective migration. *Proc. Natl. Acad. Sci.* **122**, e2423774122 (2025).
34. Ni, B. *et al.* Evolutionary Remodeling of Bacterial Motility Checkpoint Control. *Cell Rep.* **18**, 866–877 (2017).
35. Liu, W., Tokuyasu, T. A., Fu, X. & Liu, C. The spatial organization of microbial communities during range expansion. *Curr. Opin. Microbiol.* **63**, 109–116 (2021).
36. Mattingly, H. & Emonet, T. A rule from bacteria to balance growth and expansion. *Nature* **575**, 602–603 (2019).
37. Arumugam, G. & Tyagi, J. Keller-Segel Chemotaxis Models: A Review. *Acta Appl. Math.* **171**, 6 (2020).
38. Neumann, S., Vladimirov, N., Krembel, A. K., Wingreen, N. S. & Sourjik, V. Imprecision of Adaptation in Escherichia coli Chemotaxis. *PLOS ONE* **9**, e84904 (2014).
39. Guerrero-Ferreira, R. C. *et al.* Alternative mechanism for bacteriophage adsorption to the motile bacterium Caulobacter crescentus. *Proc. Natl. Acad. Sci.* **108**, 9963–9968 (2011).
40. Gonzalez, F., Helm, R. F., Broadway, K. M. & Scharf, B. E. More than Rotating Flagella: Lipopolysaccharide as a Secondary Receptor for Flagellotropic Phage 7-7-1. *J. Bacteriol.* **200**, e00363-18 (2018).
41. Ostenfeld, L. J. *et al.* A hybrid receptor binding protein enables phage F341 infection of Campylobacter by binding to flagella and lipooligosaccharides. *Front. Microbiol.* **15**, (2024).
42. Hardy, J. M. *et al.* The architecture and stabilisation of flagellotropic tailed bacteriophages. *Nat. Commun.* **11**, 3748 (2020).

678 43. Phothaworn, P. *et al.* Characterization of Flagellotropic, Chi-Like Salmonella Phages Isolated
679 from Thai Poultry Farms. *Viruses* **11**, 520 (2019).
680 44. Keegstra, J. M. *et al.* Risk–reward trade-off during carbon starvation generates dichotomy in
681 motility endurance among marine bacteria. *Nat. Microbiol.* **10**, 1393–1403 (2025).
682 45. Esteves, N. C., Porwollik, S., McClelland, M. & Scharf, B. E. The Multidrug Efflux System
683 AcrABZ-TolC Is Essential for Infection of Salmonella Typhimurium by the Flagellum-
684 Dependent Bacteriophage Chi. *J. Virol.* **95**, 10.1128/jvi.00394-21 (2021).
685 46. Esteves, N. C., Bigham, D. N. & Scharf, B. E. Phages on filaments: A genetic screen
686 elucidates the complex interactions between Salmonella enterica flagellin and bacteriophage
687 Chi. *PLOS Pathog.* **19**, e1011537 (2023).
688 47. Girgis, H. S., Liu, Y., Ryu, W. S. & Tavazoie, S. A Comprehensive Genetic Characterization
689 of Bacterial Motility. *PLoS Genet.* **3**, e154 (2007).
690 48. Yu, F. & Mizushima, S. Roles of lipopolysaccharide and outer membrane protein OmpC of
691 Escherichia coli K-12 in the receptor function for bacteriophage T4. *J. Bacteriol.* **151**, 718–
692 722 (1982).
693 49. Washizaki, A., Yonesaki, T. & Otsuka, Y. Characterization of the interactions between
694 Escherichia coli receptors, LPS and OmpC, and bacteriophage T4 long tail fibers.
695 *MicrobiologyOpen* **5**, 1003–1015 (2016).
696 50. Spöring, I. *et al.* Regulation of Flagellum Biosynthesis in Response to Cell Envelope Stress
697 in Salmonella enterica Serovar Typhimurium. *mBio* **9**, 10.1128/mbio.00736-17 (2018).
698 51. Frahm, M. *et al.* Efficiency of Conditionally Attenuated Salmonella enterica Serovar
699 Typhimurium in Bacterium-Mediated Tumor Therapy. *mBio* **6**, 10.1128/mbio.00254-15
700 (2015).
701 52. Burmeister, A. R. *et al.* Pleiotropy complicates a trade-off between phage resistance and
702 antibiotic resistance. *Proc. Natl. Acad. Sci.* **117**, 11207–11216 (2020).
703 53. Zhou, W. *et al.* Genomic Changes and Genetic Divergence of Vibrio alginolyticus Under
704 Phage Infection Stress Revealed by Whole-Genome Sequencing and Resequencing. *Front.*
705 *Microbiol.* **12**, (2021).
706 54. Kargeti, M. *et al.* Experimental evolution partially restores functionality of bacterial chemotaxis
707 network with reduced number of components. *PLOS Genet.* **21**, e1011784 (2025).
708 55. Mattingly, H. H., Kamino, K., Machta, B. B. & Emonet, T. Escherichia coli chemotaxis is
709 information limited. *Nat. Phys.* **17**, 1426–1431 (2021).
710 56. Metcalf, W. W. *et al.* Conditionally replicative and conjugative plasmids carrying lacZ alpha
711 for cloning, mutagenesis, and allele replacement in bacteria. *Plasmid* **35**, 1–13 (1996).

712 57. Suprun, M. & Suárez-Fariñas, M. PlateDesigner: a web-based application for the design of
713 microplate experiments. *Bioinformatics* **35**, 1605–1607 (2019).
714